

# Effects of short-range electron-electron interactions in doped graphene

Faluke Aikebaier, Anna Pertsova, and Carlo M. Canali

*Department of Physics and Electrical Engineering, Linnaeus University, Kalmar, Sweden*

We study theoretically the effects of short-range electron-electron interactions on the electronic structure of graphene, in the presence of single substitutional impurities. Our computational approach is based on the  $\pi$  orbital tight-binding approximation for graphene, with the electron-electron interactions treated self-consistently at the level of the mean-field Hubbard model. We compare explicitly non-interacting and interacting cases with varying interaction strength and impurity potential strength. We focus in particular on the interaction-induced modifications in the local density of states around the impurity, which is a quantity that can be directly probed by scanning tunneling spectroscopy of doped graphene. We find that the resonant character of the impurity states near the Fermi level is enhanced by the interactions. Furthermore, the size of the energy gap, which opens up at high-symmetry points of the Brillouin zone of the supercell upon doping, is significantly affected by the interactions. The details of this effect depend subtly on the supercell geometry. We use a perturbative model to explain these features and find quantitative agreement with numerical results.

PACS numbers: 73.22.Pr,71.55.-i,31.15.aq,71.10.Fd

## I. INTRODUCTION

Graphene – a two-dimensional allotrope of carbon, has attracted considerable attention in recent years, largely due to its remarkable electronic properties stemming from the massless-Dirac-fermion nature of its low-energy quasiparticle states.<sup>1</sup> Most of the electronic properties of graphene that have been studied experimentally can be well described by non-interacting single-particle theory. However, electron-electron interactions in graphene are expected to be strong. In undoped clean graphene, the density of states at the Fermi level vanishes and therefore the Coulomb potential is not screened.<sup>2,3</sup> Recent experiments have shown that unscreened Coulomb interactions lead to reshaping of the ideal conical energy dispersion expected in graphene.<sup>4</sup> More precisely, the Fermi velocity near the Dirac point acquires a logarithmic correction as a result of interactions.

From a theoretical viewpoint, it can be shown that this logarithmic enhancement arises from the non-local exchange interaction, already at the level of the first-order Hartree-Fock perturbation theory.<sup>5</sup> Hence, it is the long-range nature of the electron-electron interactions in graphene that is responsible for the logarithmic correction, the most striking interaction effect observed so far in this material in the absence of external magnetic fields. As a result, theoretical work has mostly focused on investigations of long-range interactions in graphene, using a variety of techniques ranging from mean field<sup>6</sup> to renormalization group approaches.<sup>7,8</sup>

It should be noted, however, that there are several important conditions that need to be satisfied in order to observe significant long-range interaction effects experimentally. It is necessary to be able to probe a wide range of carrier concentrations and to tune the Fermi level sufficiently close the Dirac point, where the renormalization of the Fermi velocity is expected to be dramatic due to the vanishing density of states. Moreover,

spurious screening effects, e.g. dielectric screening from the substrate, should be avoided. This makes undoped high-quality suspended graphene an ideal platform for studying the effects of long-range electron-electron interactions.<sup>4</sup> On the contrary, in the case of graphene on a substrate or in the presence of disorder and impurities these effects are less relevant.

In particular, doping introduces a finite density of states at the Dirac point of graphene and the long-range part of the Coulomb potential is screened. In this case, short-range interactions become crucial. If these interactions are fairly strong, they can lead to interesting effects on the electronic structure, especially on the impurity states in the vicinity of the Fermi level. In fact, estimates of the on-site Hubbard  $U$  parameter in carbon-based molecules<sup>9,10</sup> suggest that the short-range Coulomb interactions among  $\pi$ -electron in graphene can be indeed quite large, i.e. of the order of 10 eV. A similar value is obtained by accurate *ab initio* calculations.<sup>11</sup>

In this paper, we study the effects of short-range electron-electron interactions on the electronic structure of doped graphene. We should note that the importance of impurity effects in graphene has been addressed in many theoretical studies.<sup>12–18</sup> A number of interesting features have been revealed, including the opening of the gap upon doping<sup>13,14</sup> and the appearance of impurity (acceptor or donor) states in the vicinity of the Fermi level.<sup>12,17</sup> There is also a great interest in addressing these properties experimentally<sup>19–21</sup> since doping graphene with impurities is one way to further explore and tune its electronic, magnetic and transport properties. However, the interplay of short-range electron-electron interactions and impurity potentials in graphene has not yet been fully explored.

We use a single-band ( $\pi$  orbital) tight-binding (TB) model to describe the electronic structure of graphene. A supercell method is employed to study the effects of finite doping. A substitutional impurity is introduced

in the TB Hamiltonian as a local modification of the on-site potential at the impurity site. Here we focus on attractive impurity potentials, mimicking nitrogen impurity atoms which are typical dopants in graphene.<sup>19</sup> The short-range interactions are described by means of the Hubbard model in the mean-field approximation, which is the simplest way of treating the many-body interacting problem. Interaction terms are introduced at each site in the TB Hamiltonian. We use a numerical self-consistent scheme to account for a redistribution of electronic charge around the impurity caused by interactions. As the output of our numerical calculations, we obtain the band structure and the local density of states (LDOS) around the impurity site. Furthermore, we calculate scanning tunneling microscopy (STM) images by integrating the LDOS over a small energy window above the Fermi level.

By using this approach, we show that short-range interactions introduce several remarkable features in the electronic structure of doped graphene. Importantly, they enhance the resonant character of states localized in real space around the impurity, which are induced in the vicinity of the Dirac point. The complex interplay between short-range interactions and impurity potential is also responsible for non-trivial gaps at high-symmetry crossing points in the band structure of graphene, in particular at the Dirac point.

The paper is organized as follows. In Sec. II we introduce our TB model and describe how the impurity potential and short-range interactions are incorporated in the Hamiltonian. We also provide some details of the self-consistent supercell calculations. Our findings are described in Sec. III. In particular, in Sec. III A we focus on the effects of interactions on the band structure of graphene and on some issues related to the supercell geometry. In Sec. III B we discuss the changes in the resonant character of the LDOS around the impurity for varying impurity potential strength and interaction strength. The comparison between the simulated STM topographies for non-interacting and interacting cases is provided. Finally, we draw some conclusions.

## II. METHODOLOGY

The second-quantized Hamiltonian for interacting electrons on a honeycomb lattice in the presence of impurity can be written as

$$H = \sum_{i\sigma} \varepsilon_i c_{i\sigma}^\dagger c_{i\sigma} + \sum_{\langle i,j \rangle \sigma} t_{ij} c_{i\sigma}^\dagger c_{j\sigma} + U_{\text{im}} c_{0\sigma}^\dagger c_{0\sigma} + U \sum_i n_{i\uparrow} n_{i\downarrow}. \quad (1)$$

Here  $c_{i\sigma}^\dagger$  and  $c_{i\sigma}$  are the creation and annihilation operators for electron on site  $i$  and with spin  $\sigma$ ;  $\varepsilon_i$  and  $t_{ij}$  are on-site energies and hopping parameters, respectively. Only hopping between nearest neighbors on the honeycomb lattice is included. We assume that the TB parameters are uniform, except for the on-site energy at the impurity site, and we use the values obtained by fit-

ting the TB band structures to density functional theory calculations, namely  $\varepsilon_i = 0$  and  $t_{ij} = -2.97$  eV.<sup>22</sup>

The third term in Eq. (1) represents the local impurity potential, with  $U_{\text{im}}$  being the impurity potential strength ( $U_{\text{im}} < 0$  for attractive impurity). In our calculations we use  $U_{\text{im}} = -10$  eV and  $U_{\text{im}} = -20$  eV in order to obtain visible trends for the impurity states in the vicinity of the Fermi level.

The last term describes the on-site interaction between two electrons with opposite spins on site  $i$  (including the impurity site), with  $U$  ( $U \geq 0$ ) being the Hubbard  $U$  parameter, which expresses the strength of the intra-atomic Coulomb repulsion. Here  $n_{i\sigma}$  is the number operator, defined as  $n_{i\sigma} = c_{i\sigma}^\dagger c_{i\sigma}$ . We consider  $U = 0$ , or non-interacting case, and  $U = 9.3$  eV, which is the value obtained for graphene using the constrained Random Phase Approximation method.<sup>11</sup> In order to extract the trends in the electronic structure with increasing the interaction strength we also use a larger value of  $U = 20$  eV.

In the mean-field approximation, the two-body interaction term in Eq. (1) becomes

$$U \sum_i n_{i\uparrow} n_{i\downarrow} = U \sum_i \left( \langle n_{i\downarrow} \rangle c_{i\uparrow}^\dagger c_{i\uparrow} + \langle n_{i\uparrow} \rangle c_{i\downarrow}^\dagger c_{i\downarrow} \right), \quad (2)$$

where  $\langle n_{i\sigma} \rangle$  is the average electron occupation number, or density, for spin-up ( $\sigma = \uparrow$ ) and spin-down ( $\sigma = \downarrow$ ) electrons. Here we consider a non spin-polarized case so that  $\langle n_{i\uparrow} \rangle = \langle n_{i\downarrow} \rangle$ .

In pristine graphene with the Fermi level exactly at the Dirac point, the average electron occupation number is a constant equal to 1/2. Adding a mean-field field on-site potential does not break the translational invariance of the crystal and the average occupation number remains constant. In fact, in orthogonal basis such a potential merely introduces a rigid shift of the energy bands (note that in non-orthogonal basis the interplay between the overlap integrals and the on-site interactions can lead to renormalization of the Fermi velocity<sup>23</sup>).

However, the presence of both mean-field on-site interactions and impurity potential can lead to non-trivial effects in the electronic structure. In this case, the potential at each site depends on the average occupation number  $\langle n_{i\sigma} \rangle$ , which is not necessarily the same on all sites. As a result, when a carbon atom is replaced by an impurity, there will be a redistribution of electronic charge in the system. In order to capture this effect, we need to perform self-consistent calculations for the Hamiltonian in Eq. (1) and (2).

At each step of the self-consistent cycle, the average occupation number for site  $i$  is calculated as

$$\langle n_{i\sigma} \rangle = \frac{1}{N} \sum_k^{\text{occ}} |b_{i\sigma}^k|^2, \quad (3)$$

where  $N$  is the number of  $k$ -points in the Brillouin zone and  $b_{i\sigma}^k$  are the coefficients in the expansions of the wavefunctions of the Hamiltonian in terms of the localized

atomic orbitals  $|i\sigma\rangle$ . These are obtained by diagonalization of the Hamiltonian at each  $k$ -point. The sum runs over all occupied states up to the Fermi level. Note that all calculations are done at half-filling.

As initial values we use the occupation numbers calculated for a non-interacting problem, i.e. for a supercell of graphene with impurity ( $U_{\text{im}} \neq 0$ ) and with  $U = 0$ . The criterion of self-consistency is

$$\sum_{i\sigma} \left| \langle n_{i\sigma} \rangle^s - \langle n_{i\sigma} \rangle^{s-1} \right| < \eta, \quad (4)$$

where  $s$  is the index of the self-consistent cycle and  $\eta$  is a small parameter (we choose  $\eta = 10^{-7}$ ). We use a linear mixing scheme, in which the input density  $\langle n_{i\sigma} \rangle_{\text{in}}^{s+1}$  at step  $s+1$  is calculated as a linear combination of outputs  $\langle n_{i\sigma} \rangle_{\text{out}}^s$  and  $\langle n_{i\sigma} \rangle_{\text{out}}^{s-1}$  from two previous steps

$$\langle n_{i\sigma} \rangle_{\text{in}}^{s+1} = (1 - \lambda) \langle n_{i\sigma} \rangle_{\text{out}}^{s-1} + \lambda \langle n_{i\sigma} \rangle_{\text{out}}^s, \quad (5)$$

where  $\lambda$  is the mixing coefficient; we use  $\lambda = 0.25$ , which allows us to achieve self-consistency in less than 100 steps.

In order to model the effect of finite impurity concentration, we construct a  $p \times p$  supercell by replicating a graphene unit cell  $p$  time along each of the two-dimensional lattice vectors [see Fig. 1(a)]. The impurity atom substitutes a carbon atom in the supercell. In this work, we use two different supercells with  $p = 6$  and  $p = 7$ . Atomic concentration of the dopants depends on the size of the supercell so the concentration is slightly different for the two choices, namely 1.0% for a  $7 \times 7$  and 1.4% for a  $6 \times 6$  supercell. It is known that for  $p = 3q$ , where  $q$  is an integer, the Dirac points of graphene,  $K$  and  $K'$ , are mapped onto the  $\Gamma$  point of the Brillouin zone of the supercell.<sup>13,24,25</sup> as illustrated in Fig. 1(b). This does not happen if  $p$  is not divisible by 3. Therefore, the  $6 \times 6$  supercell is special. As we explain in Sec. III A, the effects of impurity potential and interactions in this case are rather non-trivial. This is the main reason for considering two different supercell sizes.

### III. RESULTS

#### A. Bandstructure

It is known that the finite amount of doping opens up an energy gap at the Dirac point of graphene.<sup>13,15,17</sup> Here we address the question of how the details of the bandstructure near the gap are affected by interactions.

We start with a special supercell geometry  $p \times p$ , with  $p$  divisible by 3 ( $p = 6$  in our calculations). Figure 2(a)-(b) shows the bandstructure of the  $6 \times 6$  supercell with impurity potential  $U_{\text{im}} = -10$  eV and  $U_{\text{im}} = -20$  eV, respectively, for three values of the interaction strength,  $U = 0$ ,  $U = 9.3$  eV and  $U = 20$  eV. Note that in the bandstructure calculations, different impurity potential and interaction strength introduce a shift of the energy bands with

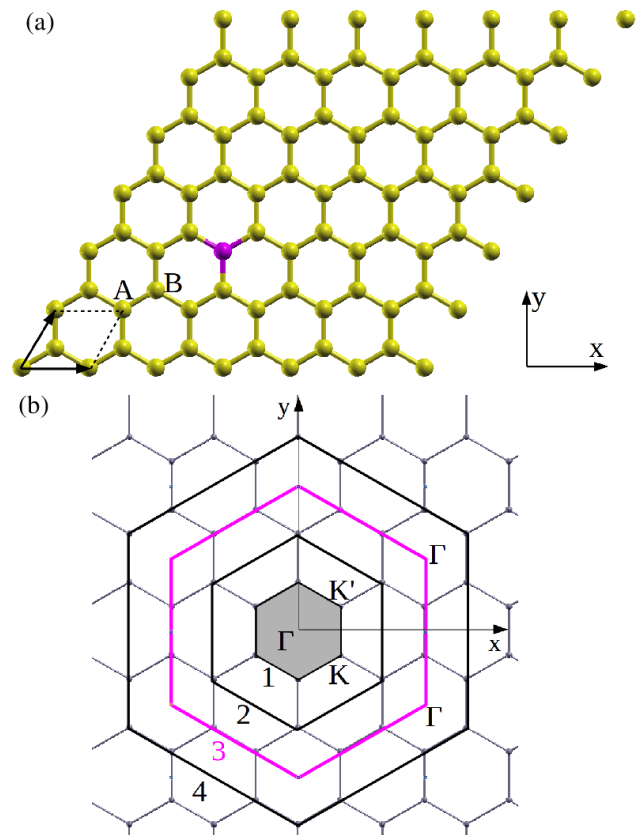


FIG. 1. (Color online) (a)  $6 \times 6$  supercell of graphene with a substitutional impurity. A magenta sphere represents the impurity atom. Dashed lines mark the unit cell of pristine graphene and arrows show the primitive lattice vectors. A and B denote carbon atoms in the two equivalent sublattices. (b) Brillouin zone folding in graphene. Shaded area (1) represents the first Brillouin zone of a  $p \times p$  supercell of graphene. Numbered curves correspond to the first Brillouin zone of the unit cell for different  $p$ :  $p = 3q - 1$  (2),  $p = 3q$  (3) and  $p = 3q + 1$ . For  $p = 3q$  the Dirac points of graphene ( $K$ ,  $K'$ ) are mapped onto  $\Gamma$  point of the folded Brillouin zone. In other cases,  $K$  and  $K'$  are mapped onto  $K$  and  $K'$  of the folded Brillouin zone.

respect to a reference case, i.e. non-interacting pristine graphene ( $U_{\text{im}} = 0$  and  $U = 0$ ). In order to examine the features around the gap for different choices of parameters, we align the position of the doubly degenerate state (see the discussion below) in all curves in Fig. 2(a)-(b) to the value found for  $U = 0$  for a given impurity potential strength.

As we mentioned before, in the case of  $p = 6$  both  $K$  and  $K'$  are mapped onto  $\Gamma$  point,<sup>13,24,25</sup> producing four degenerate states at  $\Gamma$  in the absence of impurities and interactions. When one carbon atom in the supercell is substituted by an impurity atom, a gap opens up between two states at  $\Gamma$ , however the other two states remain degenerate. More precisely, for  $U = 0$  three of the four states at  $\Gamma$  are degenerate while one of the states moves away from the Dirac point. This situation is referred to

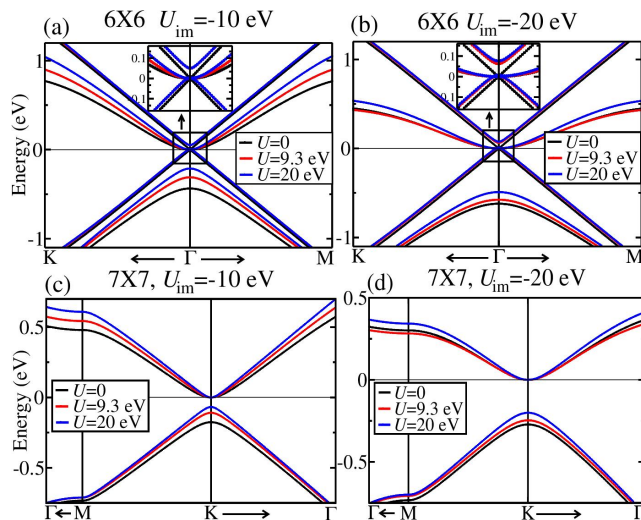


FIG. 2. (Color online) Bandstructure of doped graphene along the high-symmetry lines of the Brillouin zone for  $6 \times 6$  (a,b) and  $7 \times 7$  (c,d) supercell, for varying impurity potential strength  $U_{\text{im}}$  and interaction strength  $U$ . Left panels are for  $U_{\text{im}} = -10$  eV, right panels for  $U_{\text{im}} = -20$  eV. In each panel three cases are shown:  $U = 0$  (black),  $U = 9.3$  eV (red) and  $U = 20$  eV (blue). Horizontal line in (a) and (b) is the position of the doubly degenerate state at  $\Gamma$ , adjusted to the value found for  $U = 0$  (see text for details). Horizontal line in (c) and (d) marks the conduction band maximum, which has been aligned with the value found for  $U = 0$ .

as the *pseudogap*<sup>13</sup> since there is still a pair of linearly dispersed states crossing at the neutrality point. Hence, effectively there is no band gap for this special supercell size.

One can clearly see from Fig. 2(a) that the size of the pseudogap decreases with increasing the interaction strength. On-site interactions cause a redistribution of charge around the impurity. We find that in the case of the attractive impurity potential  $U_{\text{im}} = -10$  eV, the total average occupation at the impurity site decreases from  $\langle n_0 \rangle = 0.89$  in the non-interacting case to  $\langle n_0 \rangle = 0.82$  for  $U = 9.3$  eV. The on-site Coulomb repulsion prevents extra charge from accumulating on the impurity and therefore the strength of the impurity potential is effectively reduced. For the impurity potential which is twice stronger, the pseudogap for the same values of  $U$  is noticeably larger [see Fig. 2(b)].

In addition to a large pseudogap, for  $U \neq 0$  there is also a smaller pseudogap which opens up at  $\Gamma$  [see the insets in Fig. 2(a)-(b)]. There are now only two generate states at  $\Gamma$ , while the other two states shift, respectively, above and below the crossing point. Interestingly, the effect of interactions on the small pseudogap is opposite to that on the large one, e.g. its value increases with increasing the interaction strength. A perturbative model described in Appendix A suggests that the smaller gap results from the contribution of the states localized on sublattice B, if we assume that the impurity is substituted in sublattice

A. Within our model, this effect is solely due to interactions (the contribution of sublattice B to the gap is zero in the absence of interactions<sup>13</sup>). We find the following values for the two gaps at  $\Gamma$  from analytical calculations (see Appendix A for details). In the non-interacting case and  $U_{\text{im}} = -10$  eV, the large pseudogap is -0.56 eV. For  $U = 9.3$  eV, the large pseudogap decreases to 0.39 eV. At the same time, a small pseudogap of 0.05 eV opens up. For  $U = 20$  eV, the large and small pseudogaps become 0.28 eV and 0.06 eV, respectively. These values are all in good agreement with the pseudogaps found in Fig. 2(a). Note that for the larger impurity potential, the trends with increasing  $U$  are the same, however for a given  $U$  both gaps are larger than in  $U_{\text{im}} = -10$  eV case. Analytical calculations using the perturbative model in this case also agree with numerical results.

Similar features are found for a regular  $7 \times 7$  supercell [see Fig. 2(c) and (d)]. Note that the conduction band minima at  $\Gamma$  have been aligned with the reference  $U = 0$  case. The main difference from the  $6 \times 6$  supercell is that in this case there is a real band gap at  $K$  ( $K'$ ). Our perturbative analysis shows that there is no contribution from sublattice B to the gap at the Dirac point, if we assumed that the impurity is substituted in sublattice A. As in the case of the  $6 \times 6$  supercell, the size of the gap decreases with increasing the interaction strength. Analytically, for  $U_{\text{im}} = -10$  eV we find a gap of 0.20 eV for  $U = 0$ , 0.14 eV for  $U = 9.3$  eV and 0.10 eV for  $U = 20$  eV. These values are in good agreement with numerical calculations. Somewhat smaller values of the gaps compared to a  $6 \times 6$  supercell for the same  $U_{\text{im}}$  and  $U$  are expected since the atomic concentration of impurities is smaller.

Bandstructure calculations presented in this section lead to a conclusion that short-range interactions effectively reduce the strength of the impurity potential, which results in a decrease of the large gap (pseudogap) at the Dirac point. In order to see how the character, e.g. the energy and the spatial extent, of the electronic states around the Dirac point is affected by interactions, we need to look at the LDOS around the impurity.

## B. Local density of states

Calculations of LDOS at the impurity site reveal several important features. A substitutional impurity introduces electronic states at energies comparable to the impurity potential ( $|U_{\text{im}}| \sim 10$  eV), i.e. far away from the Fermi level. However, there are also states appearing in the vicinity (within  $\sim 1$  eV) of the Fermi level.<sup>12,13,26,27</sup> These states are the most relevant for the low-energy electronic properties of graphene and will be examined in detail.

Figure 3 shows the double- or multi-peak impurity resonances close to the Fermi level for the  $6 \times 6$  and  $7 \times 7$  supercells, respectively, for different impurity potential and interaction strengths. The multi-peak structure of

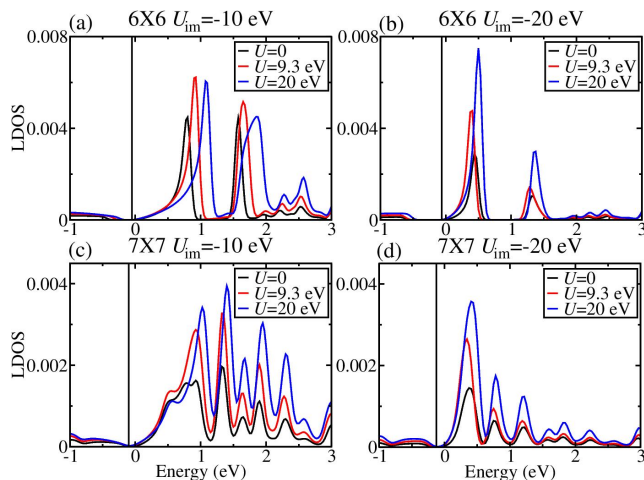


FIG. 3. (Color online) LDOS of doped graphene at the impurity site for  $6 \times 6$  (a,b) and  $7 \times 7$  (c,d) supercell, for varying impurity potential strength  $U_{\text{im}}$  and interaction strength  $U$ . Left panels are for  $U_{\text{im}} = -10$  eV, right panels for  $U_{\text{im}} = -20$  eV. In each panel three cases are shown:  $U = 0$  (black),  $U = 9.3$  eV (red) and  $U = 20$  eV (blue). Vertical lines mark the position of the Fermi level (see text for details).

the impurity resonances most likely originate from the long-range interaction, or interference, between the impurity potentials, caused by the periodicity of the supercell geometry.<sup>13</sup>

With increasing the impurity potential strength, the resonant peaks move closer to low energies. This is very similar to the case of strong potential impurities on the surface of a topological insulator.<sup>28</sup> As shown in Fig. 3(a) and (b) with  $U = 0$ , the double-peak resonance in the  $6 \times 6$  supercell approaches the Fermi level as  $U_{\text{im}}$  increases. At the same time its amplitude decreases. This finding is in agreement with semi-analytical calculations in Refs. 12, 26, and 27. The effect of the impurity potential is more striking in the case of a regular  $7 \times 7$  supercell [Fig. 3(c) and (d)]. In this case, in addition to shifting the peaks to lower energies, a stronger impurity potential  $U_{\text{im}} = -20$  eV also makes the peaks narrower, thus enhancing their resonant character [see in particular the first peak in Fig. 3(c) and (d) with  $U = 0$ ].

In the interacting case, the amplitude of the resonances increases with  $U$ . This can be seen in all panels in Fig. 3 with  $U = 9.3$  eV and  $U = 20$  eV, with the exception of the  $6 \times 6$  supercell with  $U_{\text{im}} = -10$  eV and  $U = 20$  eV, where the amplitude of the peak decreases slightly. In the case of  $U_{\text{im}} = -10$  eV, for both supercells the impurity resonances move further away from the Fermi level with increasing  $U$ . This is perfectly consistent with our observations for the non-interacting case with decreasing impurity potential. However, in the case of a very large impurity potential  $U_{\text{im}} = -20$  eV, the trend in the position of the resonances is less obvious. The peaks either do not move appreciably as in the case of  $U = 20$  eV or even seem to move slightly towards the low-energy re-

gion for  $U = 9.3$  eV. Below we elaborate more on these findings.

Increasing  $U$  reduces the overall strength of the impurity potential, which is confirmed by decrease of the energy gap at the Dirac point due to the presence of impurities (Sec. III A). However, short-range electron-electron interactions controlled by  $U$  do not only change the potential directly at the impurity site but also affect the on-site potential and the charge density around the impurity (primarily nearest and next-nearest neighbors of the impurity atom). Hence, both the amplitude and the spatial extent of the impurity potential is modified by interactions. Let us assume that an attractive impurity can be described by a delta-function potential well. When interactions are included, the shape of the impurity potential is smoothed out (it acquires, say, a Gaussian shape). Therefore, although the strength of the potential is reduced by a certain amount with increasing  $U$ , the potential can become more long-ranged (in a certain parameter space). This, in turn, will increase the overlap of the potentials from neighboring cells and enhance the inter-supercell interaction.

This seems to be the situation for  $U_{\text{im}} = -20$  eV and  $U = 9.3$  eV, for both choices of the supercell. In this case, the impurity potential decreases slightly due to interactions ( $U < U_{\text{im}}$ ), leading to a small decrease of the gap at the Dirac point compared to  $U = 0$  case [Fig. 2(b) and (d)]. At the same time, we find a significant difference between the average occupation numbers of the nearest and next-nearest neighbors for  $U = 0$  and  $U = 9.3$  eV (this can be also partly seen in the STM images in Fig. 5(a)-(b) and (d)-(e), for states in a small energy window above the Fermi level, where the neighbors of the impurity site appear brighter in the  $U = 9.3$  eV case compared to  $U = 0$ ). As a result, the amplitude of impurity resonances in LDOS increases but their position shifts to lower energies.

In contrast to this, for  $U_{\text{im}} = -20$  eV and  $U = 20$  eV, the average occupation numbers of the nearest and next-nearest neighbors of the impurity site do not change appreciably compared to  $U = 0$  case. The strength of the impurity potential for this value of  $U$  is significantly reduced, leading to a large decrease of the energy gap [Fig. 2(b) and (d)]. As a result, the amplitude of impurity resonances increases further, however their position remain close to the  $U = 0$  value. These features strongly suggest that the position of the impurity resonances is sensitive to the spatial extent of the impurity potential, namely the resonances move closer to zero energy when the potential becomes more long-ranged.

To further clarify the changes in the intensity and the spatial character of the low-energy impurity peaks, brought about by interactions, we present the simulated STM topographies in Fig. 4 and Fig. 5 for  $U_{\text{im}} = -10$  eV and  $U_{\text{im}} = -20$  eV, respectively. For this we plot LDOS for each atom in the supercell,<sup>29</sup> integrated over the energy window  $\Delta E$  above the Fermi level (we choose  $\Delta E = 0.25$  eV). This gives an estimate of the tunnel-

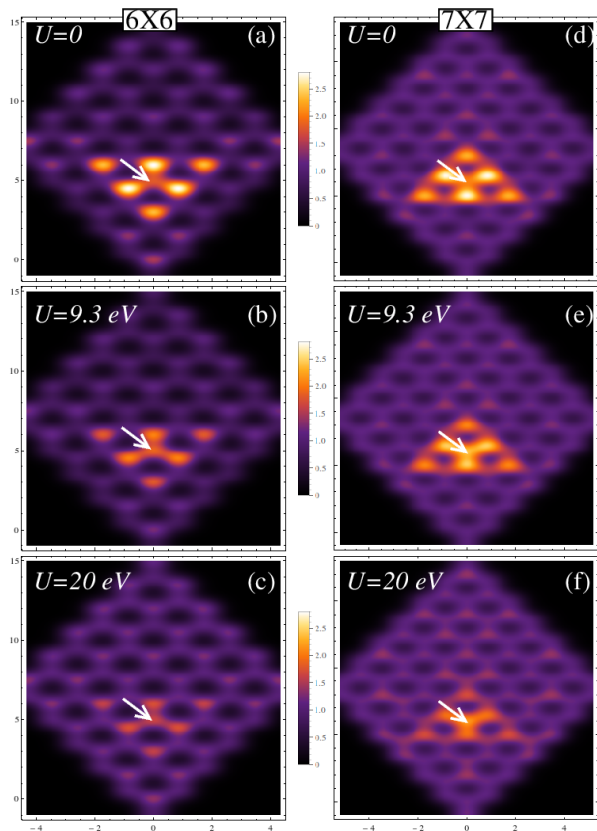


FIG. 4. (Color online) Simulated STM topographies (LDOS for all atoms in the supercell) for  $6 \times 6$  (left panels) and  $7 \times 7$  (right panels) supercell, for a fixed impurity potential strength  $U_{\text{im}} = -10$  eV and varying interaction strength:  $U = 0$  (a,d),  $U = 9.3$  eV (b,e) and  $U = 20$  eV (c,f). Arrows mark the position of the impurity atom. Note the logarithmic color scale.

ing current as electrons tunnel out of the occupied states of the STM tip into the unoccupied states of graphene. The increase of the electronic density of states in this energy window gives rise to a bright triangular feature around the impurity. Note that for the  $6 \times 6$  supercell the impurity is located in sublattice A, while for the  $7 \times 7$  supercell it is located in sublattice B. Therefore the bright triangular features in the two supercells appear rotated by  $180^\circ$  with respect to each other.

The difference between non-interacting and interacting cases is clearly visible in the STM images. In all cases considered, the impurity site becomes progressively brighter compared to its neighbors with increasing  $U$ . This means that the electronic states in the small energy window above the Fermi level become more localized on the impurity site as a result of interactions. This is most evident in the case of the  $7 \times 7$  supercell [Fig. 4(d)-(f)]. For  $U_{\text{im}} = -10$  eV, the overall intensity of the images decreases with  $U$ . For a stronger  $U_{\text{im}} = -20$  eV impurity potential, the trend is similar with the exception of the intermediate interaction strength  $U = 9.3$  eV. In this case, the contribution of the nearest and next-nearest

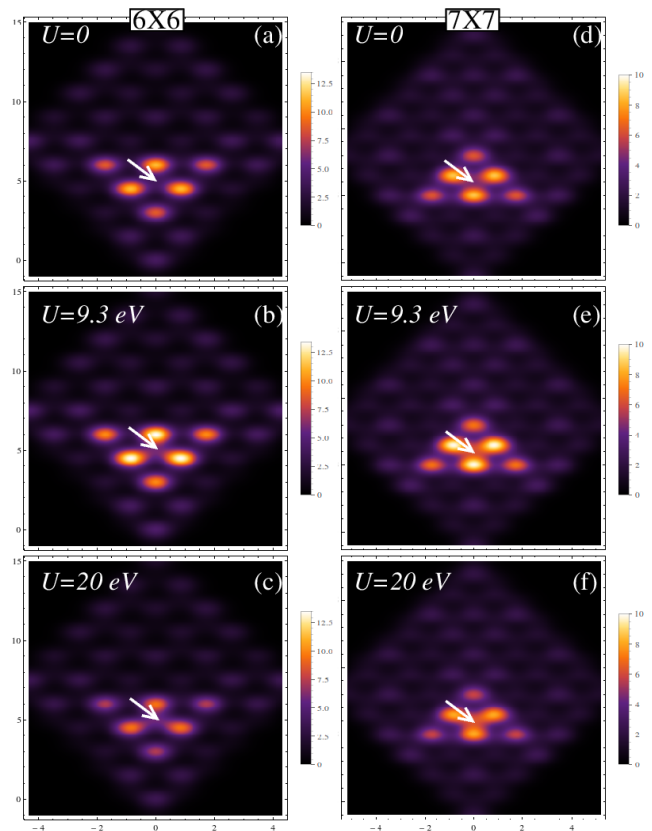


FIG. 5. (Color online) Same as Fig. 4 but with impurity potential strength  $U_{\text{im}} = -20$  eV.

neighbors is even stronger than in the  $U = 0$  case. This correlates with the corresponding features in the LDOS discussed above.

#### IV. CONCLUSIONS

We have presented a theoretical study of the effects of electron-electron interactions on the electronic states of graphene in the presence of substitutional impurities. Using a self-consistent TB model with on-site interactions treated at the mean-field level, we have shown that the size of the gap, which opens up at the Dirac point in graphene upon doping, and the character of the low-energy electronic states are modified by interactions. The mechanism for these effects is provided by the interplay between the impurity potential and the on-site repulsion, which leads to significant re-arrangement of the electronic charge around the impurity compared to the non-interacting case.

In particular, we found that the size of the gap decreases with increasing the interaction strength. Intuitively, this can be understood as follows. In the case of an attractive impurity potential, which mimics nitrogen dopants in graphene, adding the on-site Coulomb repulsion effectively reduces the strength of the potential, i.e.

the depth of the potential well decreases. This is due to the fact the on-site repulsion prevents extra electronic charge from accumulating on the impurity site.

For a special supercell size  $p \times p$ , where  $p$  is divisible by 3, both  $K$  and  $K'$  are mapped onto  $\Gamma$  point of the folded Brillouin zone. Therefore, in the case of undoped non-interacting graphene, there are four degenerate states at the neutrality point. It is known that when the impurity potential is included, a gap (pseudogap) opens up between two of these states while the other pair remains degenerate.<sup>13</sup> We have shown that the size of this pseudogap is reduced by interactions. Interestingly, in addition to this, a small gap opens up between the second pair of states at the  $\Gamma$  point, which are otherwise degenerate in the absence of interactions. We explain these features both qualitatively and quantitatively, using a perturbative model based on the generalization of the approach developed by Lambin *et al.*<sup>13</sup> to the interacting case.

Furthermore, we have studied the behavior of the impurity-induced electronic states with and without interactions. There are two groups of states which can be detected in the density of states when a carbon atom in the supercell is replaced by an impurity atom. First, there are states which emerge far away from the Fermi energy, with their energies of the same order of magnitude as the impurity potential ( $\approx 10$  eV in our calculations). Second, there are states appearing close to the Fermi energy and are therefore of particular interest. Although the way the electron-electron interactions affect the LDOS at low energies in general depends on the impurity concentration, we found clear trends in the behavior of the impurity-resonances as both parameters, i.e. the interaction strength and the impurity potential strength, are modified.

Regardless of the interactions, the impurity levels move closer to the low-energy region (e.g. to the original Dirac point) with increasing the impurity potential strength. This finding is consistent with previous calculations for graphene.<sup>12,26,27</sup> Similar result was found in another class of Dirac materials, namely in three-dimensional topological insulators in the presence of strong potential impurities on the surface.<sup>28,30</sup> However, our self-consistent calculations for graphene in the presence of both impurities and interactions reveal novel features. For a fixed impurity potential, short-range interactions tend to enhance the amplitude of the impurity-resonances in the vicinity of the Fermi level. The position of the resonances is also affected by the spatial extent of the effective impurity potential, which is modified by interactions. As the interaction strength increases, the states become more localized on the impurity atom. The differences in the spatial distribution of the low-energy impurity states in the non-interacting and interacting cases are clearly detectable in the simulated STM topographies.

## Appendix A: Band gap in doped graphene supercell in the presence of interactions

We use a simple perturbative model, based on the model proposed in Ref. 13 for non-interacting graphene, to explain how the impurity potential and electron-electron interactions affect the band structure of doped graphene.

We first review this model for the non-interacting case with impurity.<sup>13</sup> The Hamiltonian for such a system can be written in Dirac's notation as

$$H = H_0 + H_1, \quad (\text{A1})$$

where  $H_0$  is the Hamiltonian of non-interacting pristine graphene

$$H_0 = \sum_u |u\rangle E_u \langle u| + \sum_{u,v} |u\rangle t_{uv} \langle v|, \quad (\text{A2})$$

and  $H_1$  is the perturbation introduced by the periodic arrangement of impurities

$$H_1 = \sum_{u \in 1} |u\rangle U_{\text{im}} \langle u|. \quad (\text{A3})$$

Here  $|u\rangle$  is the atomic orbital associated with site  $u$  ( $\langle u|u'\rangle = \delta_{uu'}$ ),  $E_u$  and  $t_{uv}$  are the on-site energies and the nearest-neighbors hopping integrals, respectively;  $U_{\text{im}}$  is the impurity potential and the sum over  $u \in 1$  refers to all impurity atoms belonging to sublattice 1, which substitute one carbon atom in each  $p \times p$  supercell.

In pristine graphene [Eq. (A2)], there are four states with zero energy, two for the two sublattices and two for the non-equivalent points  $K$  and  $K'$  in the Brillouin zone (we omit the spin indices for simplicity). The corresponding Bloch functions can be written as

$$|K^{A(B)}\rangle = \frac{1}{\sqrt{N_{A(B)}}} \sum_{u \in A(B)} e^{i\mathbf{K}\cdot\mathbf{u}} |u\rangle, \quad (\text{A4})$$

where  $\mathbf{K}$  is a vector in the reciprocal space corresponding to either  $K$  or  $K'$ ,  $\mathbf{u}$  is the position of site  $u$  in real space, and  $N_{A(B)}$  is the number of atoms in sublattice A(B).

The task is to calculate the first order corrections to the energy states at the Dirac point due to the impurity potential, by using degenerate state perturbation theory. Let us assume that the impurity is substituted in sublattice A. Then the states  $|K^B\rangle$  and  $|K'^B\rangle$  have zero amplitudes on atoms in sublattice A and these states are eigenstates of zero energy. Therefore, we only need to consider the subspace of degenerate eigenstates formed by the states  $|K^A\rangle$  and  $|K'^A\rangle$ . We use Eq. (A3) and Eq. (A4) to calculate the following matrix elements

$$V_{11} = \langle K^A | H_1 | K^A \rangle = \frac{U_{\text{im}}}{N_A} = \frac{U_{\text{im}}}{p^2}, \quad (\text{A5})$$

$$V_{22} = \langle K'^A | H_1 | K'^A \rangle = V_{11} = \frac{U_{\text{im}}}{p^2}, \quad (\text{A6})$$

$$\begin{aligned}
V_{12} &= \langle K^A | H_1 | K'^A \rangle = \frac{1}{N_A} \sum_{u \in 1} e^{i(\mathbf{K}' - \mathbf{K}) \cdot \mathbf{u}} \\
&= \frac{U_{\text{im}}}{p^2} \delta_{\mathbf{K}' - \mathbf{K}, \mathbf{G}}, \quad (\text{A7})
\end{aligned}$$

$$V_{21} = \langle K'^A | H_1 | K^A \rangle = V_{12} = \frac{U_{\text{im}}}{p^2} \delta_{\mathbf{K}' - \mathbf{K}, \mathbf{G}}, \quad (\text{A8})$$

where  $N_A = p^2$  since for  $p \times p$  supercell, we have  $N = 2p^2$  atoms and  $N_A = N_B = p^2$  atoms in each sublattice.  $V_{12}(V_{21})$  in Eq. (A7) is not zero only when the vector  $\mathbf{K}' - \mathbf{K}$  is equal to the reciprocal lattice vector  $\mathbf{G}$ . This condition is satisfied only if  $p$  is divisible by 3, i.e. if  $p = 3q$ , where  $p, q$  are integers. This is essentially the result obtained in Ref. 13 and it is confirmed by our calculations presented in Fig. 2 for  $U = 0$  case.

The first order corrections  $E^{(1)}$  to the energy states are then given by the eigenvalues of matrix  $V$ , with matrix elements  $V_{ij}$  ( $i, j = 1, 2$ ) defined above. This gives  $E^{(1)} = 0$  and  $E^{(1)} = 2U_{\text{im}}/p^2$  if  $p = 3q$ , and  $E^{(1)} = U_{\text{im}}/p^2$  if  $p \neq 3q$ . Hence, in the case when  $p$  is divisible by 3, all four states are mapped onto  $\Gamma$  point. Three of these states, two of which are localized on sublattice B and one on sublattice A, have zero energy. The remaining state is shifted down in energy by  $2U_{\text{im}}/p^2$  ( $U_{\text{im}} < 0$  for attractive impurity), producing a pseudogap of magnitude  $2U_{\text{im}}/p^2$ . This is exactly the situation shown in Fig. 2(a) and (b) for the  $6 \times 6$  supercell. In the case when  $p$  is not divisible by 3, the degeneracy between  $K$  and  $K'$  is lifted and there are now two states at each of these points, separated by a gap of  $U_{\text{im}}/p^2$ . This is the situation for the  $7 \times 7$  supercell in Fig. 2(c) and (d).

Combining the results for  $p = 3q$  and  $p \neq 3q$ , to the lowest order in the perturbation theory the gap (pseudogap) induced by the impurity potential can be written as

$$E_{\text{gap}} = \frac{U_{\text{im}}}{p^2} + \frac{U_{\text{im}}}{p^2} \delta_{\mathbf{K}' - \mathbf{K}, \mathbf{G}}. \quad (\text{A9})$$

For  $U_{\text{im}} = -10$  eV,  $E_{\text{gap}} = -0.56$  eV if  $p = 6$  and  $E_{\text{gap}} = -0.2$  eV if  $p = 7$ . These values coincide with the gaps found numerically [see Fig. 2(a) and (c) with  $U = 0$ ].

Below we extend this model to the interacting case. The Hamiltonian of the interacting system can be written as

$$H = H_0 + H_1 + H_2, \quad (\text{A10})$$

where  $H_0$  and  $H_1$  are given by Eq. (A2) and Eq. (A3), respectively, and  $H_2$  is the perturbation introduced by short-range interactions which is given by

$$H_2 = \sum_u |u\rangle (U \cdot \langle n_{u\sigma} \rangle) \langle u|. \quad (\text{A11})$$

In accordance with Eq. (2),  $\langle n_{u\sigma} \rangle$  is the average electron occupation number on site  $u$  corresponding to spin  $\sigma$ . When the mean-field interaction term is included, the energy bands acquire a rigid shift. In order to compare

the results to the non-interacting case, we need to subtract this shift. Let us assume that it is proportional to an average quantity  $\langle \bar{n}_{u\sigma} \rangle$ , which is a constant. Then the energy that needs to be subtracted is  $U \cdot \langle \bar{n}_{u\sigma} \rangle$ .

We now calculate the first-order corrections to the energy states at the Dirac point due to interactions using the same procedure. Since the sum in Eq. (A11) can be decomposed into the sum over  $u \in A$  and the sum over  $u \in B$ , we can calculate corrections due to these two terms separately. For each of them we need to consider either the subspace formed by the states  $K^A$  and  $K'^A$ , or by the states  $K^B$  and  $K'^B$ . Let us assume for simplicity that all occupation numbers for atoms in sublattice A are approximately the same and equal to  $\langle \bar{n}_{u\sigma} \rangle$ , except for the impurity site. Then the corresponding matrix elements are given by

$$\begin{aligned}
W_{11}^A &= \langle K^A | H_2 | K^A \rangle = \frac{1}{2N_A} \sum_{u \in A, \sigma} U (\langle n_{u\sigma} \rangle - \langle \bar{n}_{u\sigma} \rangle) \\
&= \frac{U}{p^2} (\langle n_{u'\sigma} \rangle - \langle \bar{n}_{u\sigma} \rangle), \quad (\text{A12})
\end{aligned}$$

$$\begin{aligned}
W_{12}^A &= \langle K^A | H_2 | K'^A \rangle \\
&= \frac{U}{p^2} (\langle n_{u'\sigma} \rangle - \langle \bar{n}_{u\sigma} \rangle) \delta_{\mathbf{K}' - \mathbf{K}, \mathbf{G}}, \quad (\text{A13})
\end{aligned}$$

$$W_{22}^A = \langle K'^A | H_2 | K'^A \rangle = W_{11}^A, \quad (\text{A14})$$

$$W_{21}^A = \langle K'^A | H_2 | K^A \rangle = W_{12}^A, \quad (\text{A15})$$

where  $u'$  is the impurity site; 2 in the denominator stands for spin. As before, first order corrections to the energy states are given by the eigenvalues of matrix  $W^A$ , with matrix elements  $W_{ij}^A$  ( $i, j = 1, 2$ ), and differ for  $p = 3q$  and  $p \neq 3q$ . These corrections give the following contribution to the energy gap at the Dirac point

$$E_{\text{gap}}^{\text{int}(A)} = \frac{U}{p^2} (\langle n_{u'\sigma} \rangle - \langle \bar{n}_{u\sigma} \rangle) (1 + \delta_{\mathbf{K}' - \mathbf{K}, \mathbf{G}}). \quad (\text{A16})$$

In a similar way, we calculate the first-order corrections in the subspace formed by states  $K^B$  and  $K'^B$ . The corresponding matrix elements are given by

$$\begin{aligned}
W_{11}^B &= \langle K^B | H_2 | K^B \rangle = \frac{1}{2N_B} \sum_{u \in B, \sigma} U (\langle n_{u\sigma} \rangle - \langle \bar{n}_{u\sigma} \rangle) \\
&= \frac{U}{p^2} \sum_{u \in \text{nn of } u'} (\langle n_{u\sigma} \rangle - \langle \bar{n}_{u\sigma} \rangle), \quad (\text{A17})
\end{aligned}$$

$$\begin{aligned}
W_{12}^B &= \langle K^B | H_2 | K'^B \rangle \\
&= \frac{U}{p^2} \sum_{u \in \text{nn of } u'} (\langle n_{u\sigma} \rangle - \langle \bar{n}_{u\sigma} \rangle) \delta_{\mathbf{K}' - \mathbf{K}, \mathbf{G}}, \quad (\text{A18})
\end{aligned}$$

$$W_{22}^B = \langle K'^B | H_2 | K'^B \rangle = W_{11}^B, \quad (\text{A19})$$

$$W_{21}^B = \langle K'^B | H_2 | K^B \rangle = W_{12}^B, \quad (\text{A20})$$

where we assumed that all atoms in sublattice B have approximately the same occupation  $\langle \bar{n}_{u\sigma} \rangle$ , except for the nearest neighbors of the impurity atom. This is a reasonable assumption since these atoms are most strongly



TABLE I. Values of band shifts and average occupation numbers used in Eq. (A22) for  $U_{\text{im}} = -10$  eV and  $U = 9.3$  eV.

Band shift	$\langle \bar{n}_{u\sigma} \rangle$	$\langle n_{u'\sigma} \rangle$ (imp.)	$\langle n_{u\sigma} \rangle$ (nn of imp.)
4.60 eV	0.49	0.82	0.46

affected by the impurity. Then the contribution to the energy gap, stemming from corrections to the states localized on sublattice B, is given by

$$E_{\text{gap}}^{\text{int(B)}} = \frac{U}{p^2} \sum_{u \in \text{nn of } u'} (\langle n_{u\sigma} \rangle - \langle \bar{n}_{u\sigma} \rangle) (1 + \delta_{\mathbf{K}' - \mathbf{K}, \mathbf{G}}). \quad (\text{A21})$$

Finally, combining the corrections due to the impurity potential [Eq. (A9)] and due to interactions [Eq. (A16) and Eq. (A21)], we obtain the expression for the energy gap at the Dirac point

$$E_{\text{gap}}^{\text{int}} = \left\{ \left( \frac{U_{\text{im}}}{p^2} + \frac{U}{p^2} (\langle n_{u'\sigma} \rangle - \langle \bar{n}_{u\sigma} \rangle) \right) (1 + \delta_{\mathbf{K}' - \mathbf{K}, \mathbf{G}}) \right\} + \left\{ \frac{U}{p^2} \sum_{u \in \text{nn of } u'} (\langle n_{u\sigma} \rangle - \langle \bar{n}_{u\sigma} \rangle) (1 + \delta_{\mathbf{K}' - \mathbf{K}, \mathbf{G}}) \right\}, \quad (\text{A22})$$

where the expression inside the first curly bracket is due to the states localized on sublattice A, while the second one is due the states localized on sublattice B.

Let us now summarize what happens to the four zero energy states, when both the impurity potential and interactions are present. When  $p = 3q$ , all four states are mapped onto  $\Gamma$  point. As one can see from Eq. (A22), one of the states, corresponding to sublattice A, remains at zero energy, while the other one shifts by  $E_{\text{gap}}^{\text{int(A)}} = 2 \left[ \frac{U_{\text{im}}}{p^2} + \frac{U}{p^2} \cdot (\langle n_{u'\sigma} \rangle - \langle \bar{n}_{u\sigma} \rangle) \right]$ . We can estimate this quantity by taking the values of the rigid band shift and the average occupation numbers for impurity and its nearest neighbors from our numerical calculations (see Table I, numbers are similar for the two supercells). For  $U_{\text{im}} = -10$  eV,  $U = 9.3$  eV and  $p = 6$ , this energy shift is negative and is equal to  $-0.39$  eV. This corresponds to the large pseudogap (below the Dirac point) that we identified in Fig. 2(a) for this choice of  $U$ . In a similar way, one of the states localized on sublattice B remains at zero energy, while the other one shifts up in energy by  $E_{\text{gap}}^{\text{int(B)}} = 2 \frac{U}{p^2} \sum_{u \in \text{nn of } u'} (\langle n_{u\sigma} \rangle - \langle \bar{n}_{u\sigma} \rangle) = 0.054$  eV. This small energy shift is identical to the small pseudogap (above the Dirac point) found in Fig. 2(a).

When  $p \neq 3$ , the degeneracy between  $K$  and  $K'$  is lifted. There are two states at each of these points, one localized on sublattice A and the other one on sublattice B. The energy gap between the states is given by  $E_{\text{gap}}^{\text{int}} = \frac{U_{\text{im}}}{p^2} + \frac{U}{p^2} \cdot (\langle n_{u'\sigma} \rangle - \langle \bar{n}_{u\sigma} \rangle) + \frac{U}{p^2} \sum_{u \in \text{nn of } u'} (\langle n_{u\sigma} \rangle - \langle \bar{n}_{u\sigma} \rangle)$ . For  $U_{\text{im}} = -10$  eV,  $U = 9.3$  eV and  $p = 7$ ,  $E_{\text{gap}}^{\text{int}} = 0.14$  eV, which is in good agreement with Fig. 2(c).

- 
- <sup>1</sup> A. H. Castro Neto, F. Guinea, N. M. R. Peres, K. S. Novoselov, and A. K. Geim, *Reviews of Modern Physics* **81**, 109 (2009).
- <sup>2</sup> A. K. Geim and A. H. MacDonald, *Physics Today* **60**, 35 (2007).
- <sup>3</sup> V. N. Kotov, B. Uchoa, V. M. Pereira, F. Guinea, and A. H. Castro Neto, *Rev. Mod. Phys.* **84**, 1067 (2012).
- <sup>4</sup> D. C. Elias, R. V. Gorbachev, A. S. Mayorov, S. V. Morozov, A. A. Zhukov, P. Blake, L. A. Ponomarenko, I. V. Grigorieva, K. S. Novoselov, F. Guinea, and A. K. Geim, *Nature Physics* **7**, 701 (2011).
- <sup>5</sup> M. I. Katsnelson, *Graphene: carbon in two dimensions* (Cambridge University Press, 2012).
- <sup>6</sup> J. Jung and A. H. MacDonald, *Phys. Rev. B* **84**, 085446 (2011).
- <sup>7</sup> J. González, F. Guinea, and M. Vozmediano, *Nuclear Physics B* **424**, 595 (1994).
- <sup>8</sup> J. González, F. Guinea, and M. A. H. Vozmediano, *Phys. Rev. B* **59**, R2474 (1999).
- <sup>9</sup> D. P. C. Parr, R. G. and I. G. Ross, *J. Chem. Phys.* **18**, 1561 (1950).
- <sup>10</sup> D. Baeriswyl, D. K. Campbell, and S. Mazumdar, *Phys. Rev. Lett.* **56**, 1509 (1986).
- <sup>11</sup> T. O. Wehling, E. Şaş ıođlu, C. Friedrich, A. I. Lichtenstein, M. I. Katsnelson, and S. Blügel, *Phys. Rev. Lett.* **106**, 236805 (2011).
- <sup>12</sup> Y. V. Skrypnik and V. M. Loktev, *Phys. Rev. B* **73**, 241402 (2006).
- <sup>13</sup> P. Lambin, H. Amara, F. Ducastelle, and L. Henrard, *Phys. Rev. B* **86**, 045448 (2012).
- <sup>14</sup> S. S. Pershoguba, Y. V. Skrypnik, and V. M. Loktev, *Phys. Rev. B* **80**, 214201 (2009).
- <sup>15</sup> S. Latil, S. Roche, D. Mayou, and J.-C. Charlier, *Phys. Rev. Lett.* **92**, 256805 (2004).
- <sup>16</sup> C. Adessi, S. Roche, and X. Blase, *Phys. Rev. B* **73**, 125414 (2006).
- <sup>17</sup> Y. Fujimoto and S. Saito, *Phys. Rev. B* **84**, 245446 (2011).
- <sup>18</sup> W. H. Brito, R. Kagimura, and R. H. Miwa, *Phys. Rev. B* **85**, 035404 (2012).
- <sup>19</sup> L. Zhao, R. He, K. T. Rim, T. Schiros, K. S. Kim, H. Zhou, C. Gutierrez, S. P. Chockalingam, C. J. Arguello, L. Plov, D. Nordlund, M. S. Hybertsen, D. R. Reichman, T. F. Heinz, P. Kim, A. Pinczuk, G. W. Flynn, and A. N. Pasupathy, *Science* **333**, 999 (2011).
- <sup>20</sup> B. Zheng, P. Hermet, and L. Henrard, *ACS Nano* **4**, 4165 (2010), pMID: 20552993.
- <sup>21</sup> F. Joucken, Y. Tison, J. Lagoute, J. Dumont, D. Cabosart, B. Zheng, V. Repain, C. Chacon, Y. Girard, A. R. Botello-Méndez, S. Rousset, R. Sporcken, J.-C. Charlier, and L. Henrard, *Phys. Rev. B* **85**, 161408 (2012).
- <sup>22</sup> S. Reich, J. Maultzsch, C. Thomsen, and P. Ordejón, *Phys. Rev. B* **66**, 035412 (2002).
- <sup>23</sup> F. Aikebaier, A. Pertsova, and C. Canali, (unpublished).
- <sup>24</sup> Y.-C. Zhou, H.-L. Zhang, and W.-Q. Deng, *Nanotechnol-*

- ogy **24**, 225705 (2013).
- <sup>25</sup> R. Martinazzo, S. Casolo, and G. F. Tantardini, Phys. Rev. B **81**, 245420 (2010).
- <sup>26</sup> V. M. Pereira, J. M. B. Lopes dos Santos, and A. H. Castro Neto, Phys. Rev. B **77**, 115109 (2008).
- <sup>27</sup> T. O. Wehling, A. V. Balatsky, M. I. Katsnelson, A. I. Lichtenstein, K. Scharnberg, and R. Wiesendanger, Phys. Rev. B **75**, 125425 (2007).
- <sup>28</sup> A. M. Black-Schaffer and A. V. Balatsky, Phys. Rev. B **85**, 121103 (2012).
- <sup>29</sup> The discrete values of LDOS at lattice points are smeared out by adding a Gaussian broadening of  $\gamma = N_{\text{atoms}}/E_{\text{mesh}}$ , where  $N_{\text{atoms}}$  is the number of atoms in the supercell and  $E_{\text{mesh}}$  is the energy mesh.
- <sup>30</sup> R. Biswas and A. Balatsky, Phys. Rev. B **81**, 233405 (2010).